Three-Body Photodissociation of Water Molecule: An Important Prebiotic Oxygen Source

Yao Chang
Dalian Institute of the Chemical Physics https://orcid.org/0000-0002-2747-8499
Yong Yu
Dalian Institute of Chemical Physics
Feng An
Nanjing University
Zijie Luo
Dalian Institute of the Chemical Physics
Donghui Quan
Eastern Kentucky University
Xia Zhang
Xinjiang Astronomical observatory
Xixi Hu
Nanjing University https://orcid.org/0000-0003-1530-3015
Qinming Li
Dalian Institute of Chemical Physics
Jiayue Yang
Dalian Institute of Chemical Physics, Chinese Academy of Sciences
Zhichao Chen
Dalian Institute of the Chemical Physics
Li Che
Dalian Maritime University
Weiqing Zhang
Dalian Institute of Chemical Physics
Guorong Wu
Dalian Institute of Chemical Physics, Chinese Academy of Sciences. https://orcid.org/0000-0002-0212-183X
Daiqian Xie
Nanjing University https://orcid.org/0000-0001-7185-7085
Michael Ashfold
University of Bristol https://orcid.org/0000-0001-5762-7048
Kaijun Yuan (kjyuan@dicp.ac.cn)
Dalian Institute of the Chemical Physics https://orcid.org/0000-0002-5108-8984

Xueming Yang
Dalian Institute of Chemical Physics https://orcid.org/0000-0001-6684-9187

Article

Keywords: Photochemistry, Vacuum Ultraviolet Photodissociation, Three-body Dissociation, Free Electron Laser, Interstellar Photochemical Models

Posted Date: January 4th, 2021

DOI: https://doi.org/10.21203/rs.3.rs-124069/v1

Version of Record: A version of this preprint was published at Nature Communications on April 30th, 2021. See the published version at https://doi.org/10.1038/s41467-021-22824-7.

Abstract

The provenance of oxygen on the Earth and other Solar planetary bodies is a fundamental issue. It has been widely accepted that the only prebiotic pathway to produce oxygen in the Earth's primitive atmosphere was via vacuum ultraviolet (VUV) photodissociation of CO_2 and subsequent two O atom recombination. Here, we provide experimental evidence of three-body dissociation (TBD) of H_2O to produce O atoms in both ^1D and ^3P states upon vacuum ultraviolet (VUV) excitation using the newly developed tunable VUV free electron laser. Experimental results show that the TBD is the dominant pathway in the VUV H_2O photochemistry at wavelengths between 90 and 107.4 nm. The relative abundance of water in the interstellar space with its exposure to intense VUV radiation suggests that the TBD of H_2O and subsequent O atoms recombination should be an important prebiotic O_2-production, which may need to be incorporated into interstellar photochemical models.

Introduction

Oxygen is the third most abundant element in the Universe, but its molecular form (O_2) is very rare. Besides on the Earth, molecular oxygen has only been detected in two interstellar clouds[1],[2], in the moons of Jupiter[3] and Saturn[4], and on Mars[5]. Geologically based arguments suggested that Earth's original atmosphere had no oxygen and was composed mostly of H_2O, CO_2, and N_2, with only small amounts of CO and H_2[6]. Therefore, how oxygen is produced in the primitive atmosphere is a fundamentally important issue in the evolution of the early primitive atmosphere. Before the emergence of the oxygen-rich atmosphere due to the "great oxidation event" (GOE) [7],[8], about 2.33 billion years ago, which allowed the Earth to evolve into a living planet, a small amount of oxygen was already present, and this was previously attributed to an abiotic formation mechanism involving photodissociation of CO_2 by vacuum ultraviolet (VUV) light, followed by three-body recombination processes[9],

$$CO_2 + h\nu \rightarrow CO + O \qquad (1)$$

$$O + O + M \rightarrow O_2 + M \qquad (2)$$

where M is a third body to carry off the excess energy in the reaction process. Direct O_2 production pathways via VUV photodissociation of CO_2[10] and dissociative electron attachment to CO_2 [11] have recently been identified. These findings provide new insights into the sources of O_2 in Earth's early atmosphere.

In contrast, photodissociation of H_2O, one of the dominant oxygen carriers[12], has long been assumed to proceed mainly to produce hydroxyl (OH) and hydrogen (H) atom primary products, and contribute limited to the O_2 production[9]. Recently, abundant molecular O_2 in the coma of comet 67P/Churyumov-Gerasimenko (one of typical solar planetary bodies), which is dominated by H_2O, CO and CO_2, has been detected[13]. Interestingly, a strong correlation between O_2 and H_2O has been identified, indicating the O_2

formation is linked to H_2O in the comet. One plausible explanation for the strong O_2-H_2O correlation would be that the O_2 is produced by radiolysis or photolysis of water, or single collisions of energetic H_2O^+ with surfaces[14]. However, the existing photochemical reaction mechanisms seem hard to predict the measured O_2 abundance[13]. Thus, the detailed O_2 production mechanism in the coma of comets is still unclear.

The photodissociation of water has been the subject of many experimental studies, which have revealed fascinating dynamics arising from strongly coupled electronic states with strikingly different potential energy surfaces (PESs)[15],[16]. Excitation to the first excited singlet ($^1B_1$) state of H_2O at wavelengths l ~160 nm results in direct O-H bond fission yielding an H atom plus a ground state hydroxyl radical, OH ($X^2\Pi$), with little internal excitation[17]-[18],[19]. The absorption cross-section to the second excited singlet ($^1A_1$) state is maximal at l ~128 nm. Excitation at these wavelengths results in a (minor) direct dissociation channel to electronically excited OH ($A^2\Sigma^+$) + H products. The major dissociation process yields ground state OH (X) + H products following non-adiabatic transitions at conical intersections (CIs) between the and state PESs at linear H–O–H and H–H–O geometries[20]-[21],[22],[23].

Additional fragmentation pathways, named three-body dissociation (TBD), become accessible energetically at shorter photolysis wavelengths, *e.g.*

$H_2O + h\nu \rightarrow O(^3P) + H + H$ (9.513 eV) (3)

$\rightarrow O(^1D) + H + H$ (11.480 eV) (4)

where the threshold energies (E_{th}) for these fragmentation channels are given in parentheses[24]. Fragmentation channel (3) has been previously detected with small quantum yields[25],[26] following photoexcitation of H_2O at the Lyman-α wavelength (l = 121.57 nm). Because of the lack of intense tunable VUV laser sources, quantitative assessment of the importance of the H_2O TBD processes in the VUV region and its role in the O_2 formation in the interstellar space has not been possible. Recent development of the new intense VUV free electron laser (FEL), at the Dalian Coherent Light Source (DCLS), has provided an exciting tool for experimental studies of molecular photochemistry throughout the entire VUV region[27]. Here we report novel studies of H_2O photochemistry in the VUV region using the DCLS and the H-atom Rydberg tagging time-of-flight (HRTOF) technique. These experiments allow quantitative determination of the relative importance of the binary dissociation and the TBD processes following photoexcitation of H_2O in the 90-110 nm region. The present results show conclusively that the H_2O TBD process is an important pathway to form oxygen in the interstellar space.

Results And Discussion

The H_2O sample is generated in a supersonic beam, with a rotational temperature estimated to be about 10 K. The H_2O molecules were photoexcited to different Rydberg states[28] (see Fig. S1 and S2 in the

Supplementary Materials (SM))). The dissociated H-atom fragments were then detected using the HRTOF technique (see Methods Section). TOF spectra of the H atoms resulting from H_2O photodissociation at l = 107.4 nm have been recorded, with the detection axis aligned parallel and perpendicular to the polarization vector of the VUV FEL radiation. Knowing both the distance travelled by the H atom from the photodissociation area to the detector and its mass, the TOF spectra can be converted into the distributions of total kinetic energy release (TKER)[29]. Using the TKER distributions obtained in the parallel and perpendicular directions, we can construct a 3-dimensional (3D) flux diagram of the H-atom fragments. Fig. 1 shows the 3D product flux diagrams in two regions of the kinetic energy with rich structures. The tall feature at low kinetic energy (Fig. 1A) shows a large product angular anisotropy, whereas the product anisotropy in the higher kinetic energy region (Fig. 1B), is rather small.

For detailed analysis and feature assignment, the TKER distributions in parallel and perpendicular directions at l = 107.4 nm are plotted in Fig. 1C, while the product TKER distribution from photodissociation of H_2O at the magic angle (with detection angle of 54.7° relative to the polarization direction) is shown in Fig. 1D. These distributions show both sharp and broad features. Using the energy conservation relationship appropriate for a binary photodissociation process,

$$E_{h\nu} + E_{int}(H_2O) = D_0(H\text{-}OH) + E_{KE}(H + OH) + E_{int}(OH) \quad (5)$$

where, $E_{int}(H_2O)$ and $E_{int}(OH)$ are the internal energies of H_2O and OH, respectively, E_{KE} is the product total kinetic energy and D_0(H-OH) is the dissociation energy of H_2O[30]. We can assign all of the sharp structures to specific ro-vibrational levels of the OH product in the X and A states formed via the binary dissociation channel, H+OH (X or A, *v, N*). In addition to these sharp structures, the TKER spectra show two broad features: one with E_{KE} £ 600 cm^{-1} that has a large angular anisotropy, and an underlying feature that spans the range of 600 £ E_{KE} £ 16000 cm^{-1} which displays a much smaller angular anisotropy. These broad features are obviously not from the binary dissociation channel, H + OH. Based on energy conservation, the maximum kinetic energy for the H-atom product from the TBD channels (3) and (4) at 107.4 nm are 16448 cm^{-1} and 580 cm^{-1}, respectively. These limits of the two TBD channels match well with the upper limits of the two broad features in the distributions (Fig. 1). Thus, the intense broad feature at E_{KE} < 600 cm^{-1} is assigned to the O (^{1}D) + 2H channel, while the broad underlying signal extending to E_{KE} ~ 16000 cm^{-1} is attributed to the O (^{3}P) + 2H products.

Given the above analysis, the product TKER distribution in Fig. 1D can be divided into three components: O (^{1}D) + 2H, O (^{3}P) + 2H and OH + H. The first two components are broad features, while the third comprises sharp structures attributable to ro-vibrational levels of the OH (A) and OH (X) products. From Fig. 1D, the O (^{1}D) + 2H channel obviously has the highest intensity in the kinetic energy less than 600 cm^{-1}, yet it has never been reported previously in H_2O photodissociation. The O (^{3}P) + 2H channel clearly makes the major contribution in the higher kinetic energy region. This indicates that the TBD is likely the dominant process following VUV photoexcitation of H_2O at 107.4 nm.

Branching ratios for the O (^{1}D) + 2H, O (^{3}P) + 2H and OH + H fragmentation channels have been estimated by simulating the TKER distribution (Fig. 1D) using the three components shown in Fig. 2. Integrating the areas under the respective distributions returns relative H atom yields for the three channels. Recognizing that two H atoms are formed in each TBD process, the relative H atom yields are used to determine the branching ratio, *e.g.* 67% at 107.4 nm for the TBD channels (Table 1).

Photodissociation of H_2O has also been investigated at eight more VUV wavelengths between 92 nm and 109 nm, and a similar data analysis procedure is applied at these photolysis wavelengths (see Fig. S3 in the SM). The branching ratios determined for the binary and TBD channels at each wavelength are listed in Table 1. At 109.0 nm, only one TBD channel (O (^{3}P) + 2H) exists because the O (^{1}D) + 2H channel is energetically not accessible. The results mean that oxygen atoms (^{1}D and ^{3}P), not OH radicals, are the major oxygen-containing products from H_2O photolysis at $\lambda < 107.4$ nm, in striking contrast to the dominant binary photofragmentation (*i.e.* H + OH) behaviour displayed by H_2O photochemistry at longer VUV wavelengths[15].

The dissociation dynamics of the two TBD channels are also quite interesting. Since the two H atoms in the water molecule are equivalent, if they dissociate simultaneously it should yield a narrow H atom kinetic energy distribution, peaking at an E_{EK} value close to half of the available energy (see Fig. S5 and S6). However, the observed distributions are much broader than the narrow distributions for a simultaneous concerted process, implying that both TBD processes are due to mostly a sequential dissociation mechanism. Possible dissociation routes for the two channels are illustrated in Fig. 3 (and more details in Fig. S7).

The conclusion that the TBD is the dominant decay process following excitation of H_2O at these VUV wavelengths could have profound implications for our understanding of the source of oxygen production. For quantitative assessment, we have calculated the fragment-dependent photodissociation rate of H_2O by using: $J_{H2O}=\int \Phi_\lambda \Gamma \sigma_\lambda d\lambda$, where Φ_λ is the solar photon flux, Γ is the fragment quantum yield, and σ_λ is the photodissociation cross section[31]. Fig. 4 collects together the wavelength dependences of the solar photon flux in the early period[32], the total photoabsorption cross sections of the parent H_2O molecule in the VUV region (90-200 nm)[33] and the production yields of O atoms at studied photolysis wavelengths. Convoluting the solar photon flux, the photoabsorption cross sections, and the production yields implies that ~21% of the photoexcitation events of H_2O will result in O atoms. Considering the water abundance in widely interstellar circumstances, like in interstellar clouds[2,3] and in the comets 67P[13,][34], oxygen production from water photolysis should be an important process. The following recombination of oxygen atoms will produce molecular oxygen.

In addition, it is well known that water photolysis has nothing to do with oxygen production in the Earth's atmosphere under equilibrium conditions due to VUV photon screening by the thick atmosphere[10,35]. However, in the earliest period of Earth, *i.e.*, the period approaching to clement conditions on the earliest Earth followed by the current Earth-Moon system formed, the surface of Earth remained quite hot (>1000

K)[35], all of the water on the Earth was vaporized to the atmosphere and part of water clouds (emitted from volcanos or delivered by carbonaceous chondrite meteorites[6]) populated at the top of the atmosphere could absorb the VUV photons and dissociate. Given [H_2O] is 10 times abundant than [CO_2] in the atmosphere during this early, chaotic period of Earth[6] (See Fig. S4 in the SM), the O-production rate from H_2O VUV photochemistry could be 3 times larger than that of CO_2 in the same VUV wavelength region, via TBD processes: $N_{H2O}(O)/N_{CO2}(O) = (J_{H2O}(O)\times[H_2O])/(J_{CO2}(O)\times[CO_2]) = \sim 3$, where $J_{H2O}(O) = \sim 5.2\times10^{-5}$ s^{-1} (Fig. 4), $J_{CO2}(O) = \sim 1.8\times10^{-4}$ s^{-1} (Fig. S8), [H_2O] and [CO_2] are the densities of H_2O and CO_2, respectively. Since the molecular oxygen generation process should be the same in the three-body recombination process (Eq. 2), this analysis implies that H_2O photochemistry might be an important prebiotic source of O_2 in Earth's early atmosphere.

From the experimental results, it seems that more than one third of O atoms produced from H_2O TBD process populate in the metastable ^1D state. The generation of O (^1D) atoms from photodissociation of H_2O in a significant amount is also very interesting because the metastable O (^1D) atom is highly reactive[36]. It can react with almost all the gases emitted into the atmosphere. For instance, the reaction of O (^1D) with methane could be a significant source of formaldehyde in the earth's primitive atmosphere[37],[38]. Thus, the production of O (^1D) atoms from the exposure of water to VUV radiation, and the subsequent reactions of these atoms, could have been important drivers in the evolution of the earliest atmosphere.

Conclusions

In the existing interstellar photochemical model, reactions (1) and (2) are the major pathways to produce prebiotic O_2. In this work, we propose an alternative prebiotic O_2 pathway: atomic oxygen production from the TBD of water, followed by oxygen recombination reactions. Recent International Ultraviolet Explorer (IUE) satellite observation of pre-main-sequence stars suggested that the nascent sun has emitted more than 10 times VUV radiation than it does today[39]. This implies that oxygen formation by VUV photoinduced TBD of H_2O is likely an important process in the coma of comets, in the interstellar clouds and even in Earth's primitive atmosphere, and thus needs to be incorporated into interstellar photochemical model. Furthermore, the TBD of H_2O may well be important for oxygen evolution in the atmospheres of all water-rich terrestrial planets[40].

Methods

The experiments employ a newly constructed apparatus for molecular photochemistry, which is centered on the vacuum ultraviolet free electron laser (VUV-FEL) beam line at the Dalian Coherent Light Source (DCLS) [27]. Briefly, the VUV-FEL facility runs in the high gain harmonic generation (HGHG) mode, in which the seed laser is injected to interact with the electron beam in the modulator (Fig. S1). The seeding pulse, in the wavelength range (λ_{seed}) 240-360 nm, can be generated from a picosecond Ti:sapphire laser pulse.

The electron beam is generated from a photocathode RF gun, and accelerated to the beam energy of ~300 MeV by 7 S-band accelerator structures, with a bunch charge of 500 pC. The micro-bunched beam is then sent through the radiator, which is tuned to the 2nd/3rd/4th harmonic of the seed wavelength, and coherent FEL radiation with wavelength $\lambda_{seed}/2$, $\lambda_{seed}/3$ or $\lambda_{seed}/4$ is emitted. Optimization of the linear accelerator yields a high quality electron beam with emittance of ~1.5 mm·mrad, energy spread of ~1‰, and pulse duration of ~1.5 ps. In this work, the VUV-FEL operates at 10 Hz, and the maximum pulse energy is >100 μJ/pulse. The output wavelength is continuously tunable in the range 50-150 nm and the typical spectral bandwidth of the VUV-FEL output is 30~50 cm^{-1}.

The high-n H atom Rydberg tagging time-of-flight (HRTOF) technique used in this work was pioneered by Welge and coworkers[41]. The key point of this technique is the 1+1' (VUV+UV) excitation of the H atom. The first step involves VUV laser excitation of the H atom from its n=1 ground state to the n=2 state by absorbing one l = 121.57 nm photon. In the second step, the H (n=2) atom is excited with a UV (l ~365 nm) photon to a high-n (n=30-80) Rydberg state. Charged species formed in the interaction region are extracted from the TOF axis by a small electric field (~20V/cm) placed across this region. Rydberg tagged neutral H atoms fly a known distance (*d* »280 mm) from the interaction region to a rotatable microchannel plate (MCP) Z-stack detector located close behind a grounded fine metal grid. After passing through the grid, the Rydberg atoms are immediately field-ionized by the electric field (~2000V/cm) applied between the grid and the front plate of the Z-stack MCP detector. The signal detected by the MCP is amplified by a fast pre-amplifier and counted by a multichannel scaler.

Declarations

Acknowledgments

The experimental work was supported by the National Natural Science Foundation of China (NSFC Center for Chemical Dynamics (Grant No. 21688102)), the National Natural Science Foundation of China (Grant Nos. 21873099, 21922306), the Strategic Priority Research Program of the Chinese Academy of Sciences (Grant No. XDB17000000), the Key Technology Team of the Chinese Academy of Sciences (Grant No. GJJSTD20190002), and the international partnership program of Chinese Academy of Sciences (No. 121421KYSB20170012). The theoretical work was supported by the National Natural Science Foundation of China (Grant Nos. 21590802, 21733006, and 91641104). MNRA is grateful for funding from the Engineering and Physical Sciences Research Council (EPSRC, EP/L005913) and to the NFSC Center for Chemical Dynamics for the award of a Visiting Fellowship.

Supplementary materials

Absorption spectrum of H_2O, experimental results at eight more VUV wavelengths, the relative abundances of gases in the early atmosphere of the Earth, the illustration of TBD pathways, electronic structure considerations, oxygen production rate for CO_2, supplementary figures and references.

Author Contributions

K.J.Y. and X.M.Y. designed the experiments. Y.C., Y.Y., Z.J.L., Q.M.L., J.Y.Y., and Z.C.C. performed the experiments. X.Z., D.H.Q., K.J.Y., M.N.R.A., L.C., W.Q.Z., G.R.W., and X.M.Y. discussed the experimental results. F.A., X.X.H., and D.Q.X. performed the theoretical calculations. K.J.Y., M.N.R.A., and X.M.Y. prepared the manuscript.

Competing interests

The authors declare no competing interests.

Table

Table 1 The branching ratios for the binary and TBD channels following H_2O photodissociation at different VUV wavelengths (nm). The maximum uncertainty on the branching ratios is ±10%.

Dissociation	Photolysis Wavelength (nm)								
Channel	109.0	107.4	106.7	105.7	101.3	98.1	96.2	94.5	92.0
TBD ($O(^1D/^3P)$+2H)	0.35	0.67	0.76	0.62	0.77	0.72	0.79	0.86	0.86
Binary Dissociation: (H+OH)	0.65	0.33	0.24	0.38	0.23	0.28	0.21	0.14	0.14

References

[1]. Goldsmith, P. F. et al. Herschel Measurements of molecular oxygen in Orion. *Astrophys. J.* **737**, 96 (2011).

[2]. Liseau, R. et al. Multi-line detection of O_2 toward ρ Ophiuchi A. *Astron. Astrophys.* **541**, A73 (2012).

[3]. Hall, D. T. et al. Detection of an oxygen atmosphere on Jupiter's moon Europa. *Nature* **373**, 677–679 (1995).

[4]. Johnson, R. E. et al. Production, ionization and redistribution of O_2 in Saturn's ring atmosphere. *Icarus* **180**, 393–402 (2006).

[5]. Barker, E. S. Detection of molecular oxygen in the martian atmosphere. *Nature* **238**, 447–448 (1972).

[6]. Zahnle, K., Schaefer, L. & Fegley, B. Earth's earliest atmospheres. *Cold Spring Harb. Perspect. Biol.* **2,** a004895 (2010).

[7]. Luo, G. M. et al. Rapid oxygenation of Earth's atmosphere 2.33 billion years ago. *Sci. Adv.* **2**, e1600134 (2016).

[8]. Holland, H. D. The oxygenation of the atmosphere and oceans. *Philos. T. R. Soc. B* **361**, 903-915 (2006).

[9]. Kasting, J. F., Liu, S. C. & Donahue, T. M. Oxygen Levels In the Prebiological Atmosphere. *J. Geophys. Res-Oc. Atm.* **84**, 3097-3107 (1979).

[10]. Lu, Z., Chang, Y. C., Yin, Q. Z., Ng, C. Y. & Jackson, W. M. Evidence for direct molecular oxygen production in CO_2 photodissociation. *Science* **346**, 61-64 (2014).

[11]. Wang, X. D., Gao, X. F., Xuan, C. J. & Tian, S. X. Dissociative electron attachment to CO_2 produces molecular oxygen. *Nat. Chem.* **8**, 258-263 (2016).

[12]. Young, E.D. Strange water in the solar system. *Science*, **317**, 211-212 (2007).

[13]. Bieler, A. et al. Abundant molecular oxygen in the coma of comet 67P/Churyumov -Gerasimenko. *Nature* **526**, 678-681 (2015).

[14]. Yao, Y. X. & Giapis, K. P. Dynamic molecular oxygen production in cometary comae. *Nat. Commun.* **8**, 15298 (2017).

[15]. Yuan, K. J., Dixon, R. N. & Yang, X. M. Photochemistry of the water molecule: adiabatic versus nonadiabatic dynamics. *Acc. Chem. Res.* **44**, 369-378 (2011).

[16]. Yuan, K. J. et al. Nonadiabatic dissociation dynamics in H_2O: competition between rotationally and nonrotationally mediated pathways. *Proc. Natl. Acad. Sci. U.S.A.* **105**, 19148-19153 (2008).

[17]. Engel, V., Schinke, R. & Staemmler, V. Photodissociation dynamics of H_2O and D_2O in the 1st absorption-band - a complete ab initio treatment. *J. Chem. Phys.* **88**, 129-148 (1988).

[18]. Brouard, M., Langford, S. R. & Manolopoulos, D. E. New trends in the state-to-state photodissociation dynamics of $H_2O(A)$. *J. Chem. Phys.* **101**, 7458-7467 (1994).

[19]. Yang, X. F., Hwang, D. W., Lin, J. J. & Yang, X. Dissociation dynamics of the water molecule on the A^1B_1 electronic surface. *J. Chem. Phys.* **113**, 10597-10604 (2000).

[20]. van Harrevelt, R. & van Hemert, M. C. Photodissociation of water. I. electronic structure calculations for the excited states. *J. Chem. Phys.* **112**, 5777-5786 (2000).

[21]. Dixon, R. N. et al. Chemical "double slits": dynamical interference of photodissociation pathways in water. *Science* **285**, 1249-1253 (1999).

[22]. Fillion, J. H. et al. Photodissociation of H_2O and D_2O in B, C, and D states (134-119 nm). Comparison between experiment and ab initio calculations. *J. Phys. Chem. A* **105**, 11414-11424 (2001).

[23]. Mordaunt, D. H., Ashfold, M. N. R. & Dixon, R. N. Dissociation dynamics of H_2O (D_2O) following photoexcitation at the lyman-alpha wavelength (121.6 nm). *J. Chem. Phys.* **100**, 7360-7375 (1994).

[24]. On the basis of thermodynamic calculations with the data available from the thermochemical network (https://atct.anl.gov) and references therein.

[25]. Harich, S. A. et al. Photodissociation of H_2O at 121.6 nm: a state-to-state dynamical picture. *J. Chem. Phys.* **113**, 10073-10090 (2000).

[26]. Slanger, T. G. & Black, G. Photodissociative channels at 1216 Å for H_2O, NH_3, and CH_4. *J. Chem. Phys.* **77**, 2432-2437 (1982).

[27]. H. L. Wang, et al., Photodissociation dynamics of H_2O at 111.5 nm by a vacuum ultraviolet free electron laser. *J. Chem. Phys.* **148**,124301 (2018).

[28]. Fillion, J. H. et al. High resolution photoabsorption and photofragment fluorescence spectroscopy of water between 10.9 and 12 eV. *J. Chem. Phys.* **120**, 6531-6541 (2004).

[29]. The total kinetic energy can be derived using the following equation, E_{KE}= , where *d* is the flying path length of H atom (*d* ≈ 28 cm) from the photodissociation region to the detector, *t* is the measured time of flight.

[30]. Boyarkin, O. V. et al. Accurate bond dissociation energy of water determined by triple-resonance vibrational spectroscopy and ab initio calculations. *Chem. Phys. Lett.* **568**, 14-20 (2013).

[31]. Heays, A. N., Bosman, A. D. & van Dishoeck, E. F. Photodissociation and photoionization of atoms and molecules of astrophysical interest. *Astron. Astrophys.* **602**, A105 (2017).

[32]. Zahnle, K. J. & Walker, J. C. G. The evolution of solar ultraviolet luminosity. *Rev. Geophys. Space Phys.* **20**, 280-292 (1982).

[33]. Lee, L. C. & Suto, M. Quantitative photoabsorption and fluorescence study of H_2O and D_2O at 50-190 nm. *Chem. Phys.* **110**, 161-169 (1986).

[34]. Hassig, M. et al. Time variability and heterogeneity in the coma of 67P/Churyumov-Gerasimenko. *Science* **347**, aaa0276 (2015).

[35]. Sleep, N. H. The Hadean-Archaean environment. *Cold Spring Harb. Perspec. Biol.* **2**, a002527 (2010).

[36]. Tachiev, G. I. & Fischer, C. F. Breit-Pauli energy levels and transition rates for nitrogen-like and oxygen-like sequences. *Astron. Astrophys.* **385**, 716-723 (2002).

[37]. Lin, J. J., Shu, J., Lee, Y. T. & Yang, X. Multiple dynamical pathways in the $O(^1D) + CH_4$ reaction: A comprehensive crossed beam study. *J. Chem. Phys.* **113**, 5287-5301 (2000).

[38]. Yung, Y. L. & Demore, W. B. *Photochemistry of Planetary Atmosphere* (Oxford Univ. Press, New York, 1999).

[39]. Zahnle, K. J., Gacesa, M. & Catling, D. C. Strange messenger: A new history of hydrogen on Earth, as told by Xenon. *Geochim. Cosmochim. Ac.* **244**, 56-85 (2019).

[40]. Zeng, L. & Sasselov, D. The effect of temperature evolution on the interior structure of H_2O-rich planets. *Astrophys. J.* **784**, 96 (2014) and references therein.

[41]. Schnieder, L. et al. Photodissociation dynamics of H_2S at 121.6 nm and a determination of the potential energy function of $SH(A^2\Sigma^+)$. *J. Chem. Phys.* **92**, 7027-7037 (1990).

[42]. van Dishoeck, E. F., Herbst, E. & Neufeld, D. A. Interstellar water chemistry: From laboratory to observations. *Chem. Rev.* **113**, 9043-9085 (2013).

[43]. Fillion, J. H. et al. Ionization yield and absorption spectra reveal superexcited Rydberg state relaxation processes in H_2O and D_2O. *J. Phys. B: At. Mol. Opt. Phys.* **36**, 2767-2776 (2003).

Figures

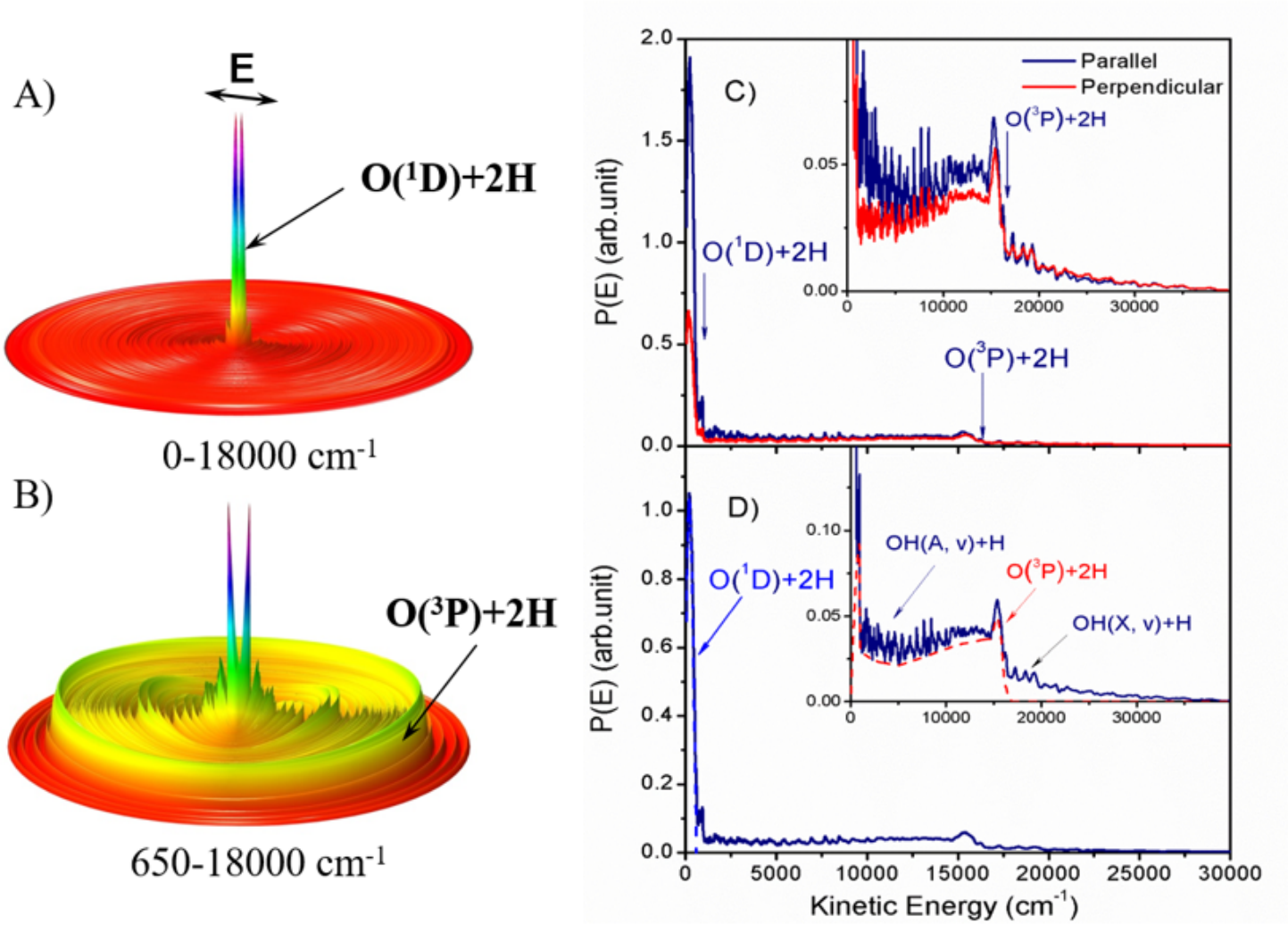

Figure 1

A) The 3D product contour diagram from the photodissociation of H2O at 107.4 nm for the total kinetic energy release (TKER) between 0 to 18,000 cm-1; B) The 3D product contour diagram for the TKER between 650 to 18,000 cm-1. C) The product TKER distributions at l = 107.4 nm with the detection axis parallel and perpendicular to the polarization vector of the VUV-FEL radiation. The energetic limits of the two TBD channels (EKEmax ~580 cm-1 and ~16448 cm-1) are marked, and the inset displays the same spectra on an expanded vertical scale. D) The product TKER distribution at l = 107.4 nm with the detection axis at 54.7o (magic angle) to the polarization direction, along with the simulated TKER distributions for the O(1D) + 2H and O(3P) + 2H TBD channels.

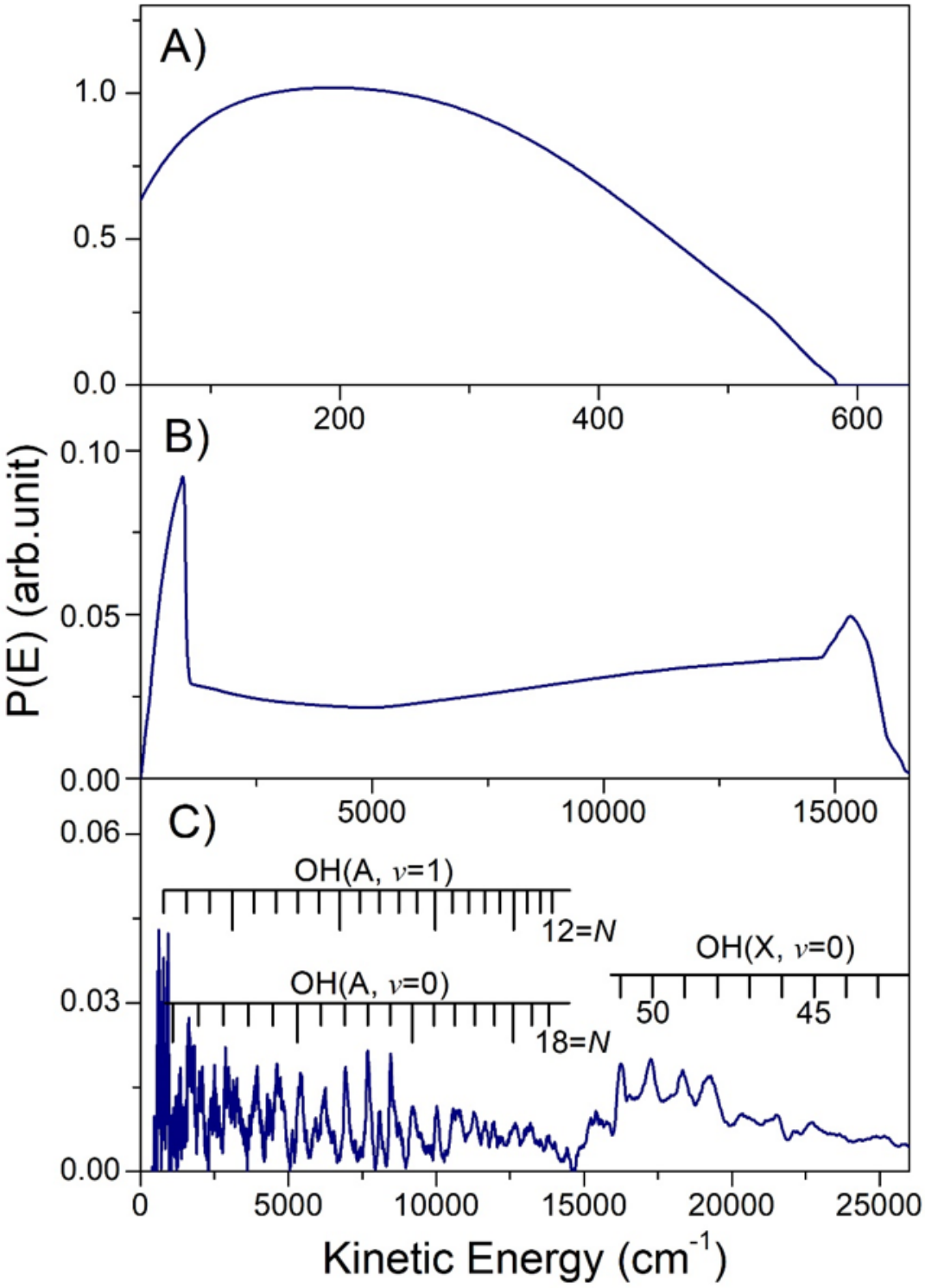

Figure 2

TKER distributions determined from simulating the (A) O(1D) + 2H, (B) O(3P) + 2H and (C) OH + H product yields from photodissociation of H2O at l = 107.4 nm. The sharp features in the H + OH product yield have been assigned to population of rovibrational levels of the X and A states of the OH radical.

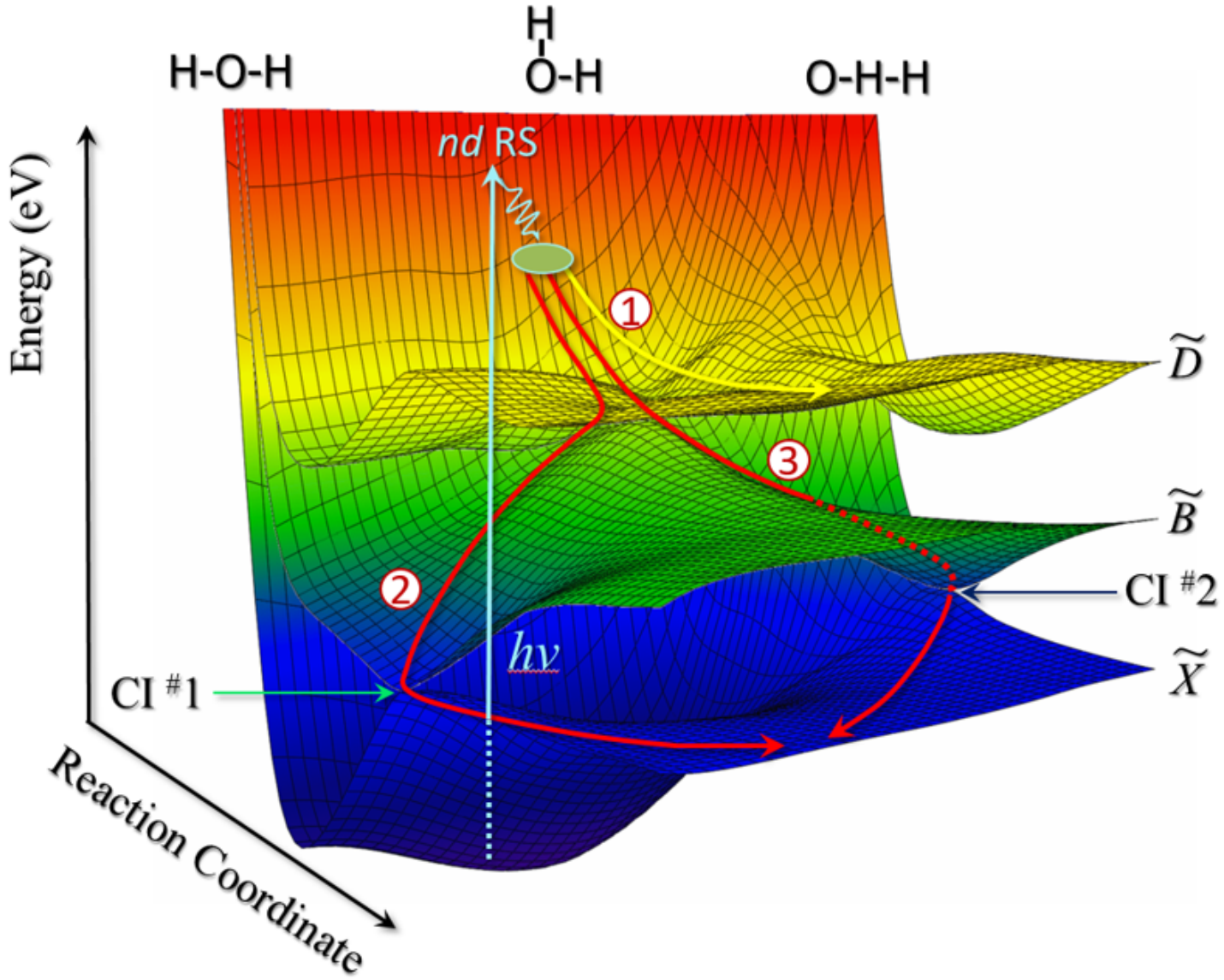

Figure 3

Illustration of the TBD mechanisms of H2O upon VUV excitation. Photoexcitation populates the nd Rydberg states (nd RS) which undergo efficient non-adiabatic coupling to the D˜ state. Path 1 illustrates the possible direct dissociation route from the D˜ state to form O(1D)+2H products. Paths 2 and 3 illustrate plausible routes for the more complicated O(3P)+2H dissociation paths: from the D˜ state to the B˜ state and then to the ground state via the two conical intersections (CI #1 or CI #2), following the initial internal conversion from the excited nd RS to the D˜ state. This picture is consistent with the observed angular anisotropy for the two channels: the O(1D)+2H channel is a more direct dissociation process with larger angular anisotropy, while the O(3P)+2H channel is a more complicated dissociation process with smaller angular anisotropy.

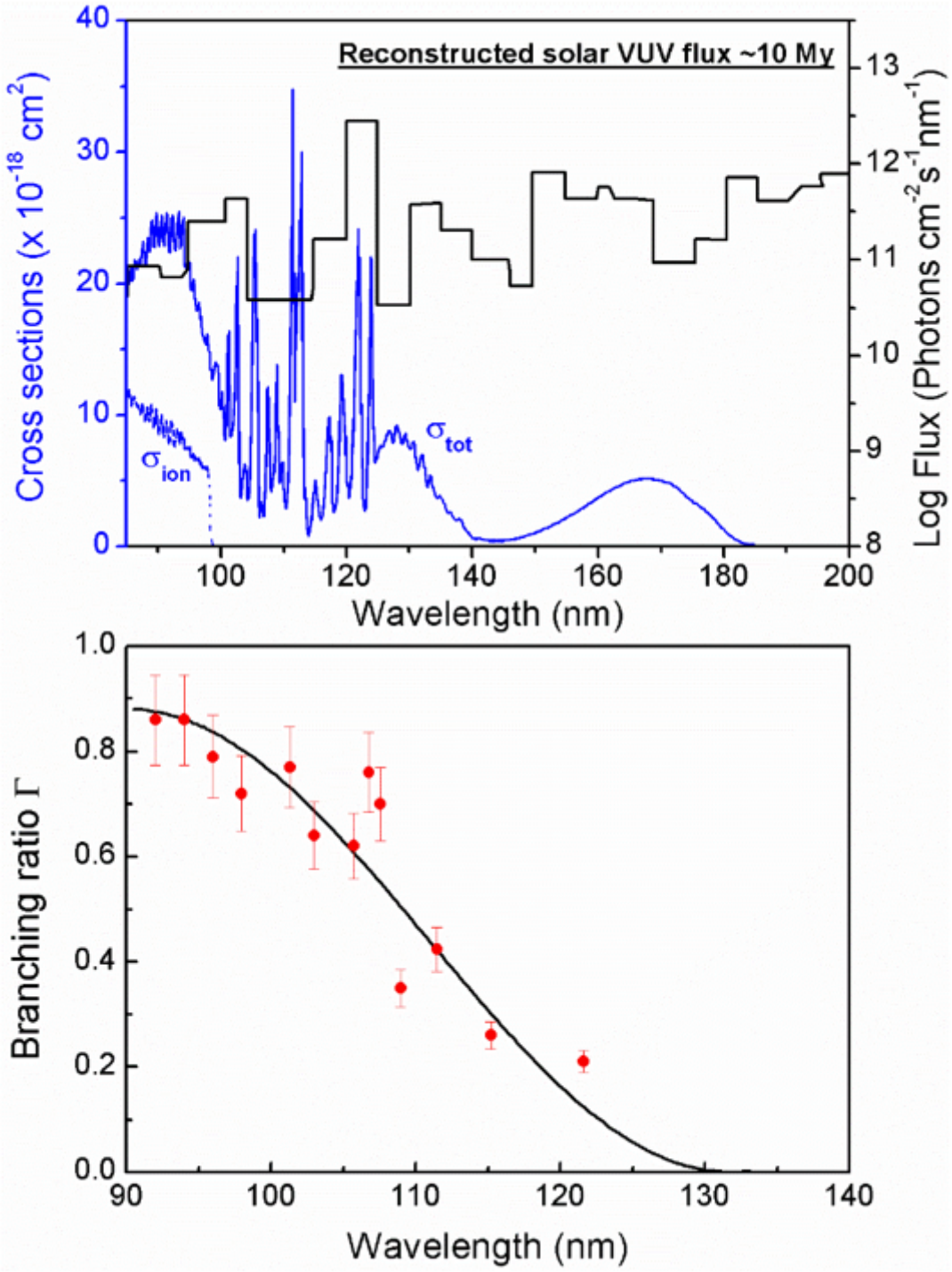

Figure 4

Plot showing the wavelength dependences of the reconstructed VUV solar flux (90-200 nm) at ~10My (10My=1×107 years, reconstructed from Ref. 32. The VUV solar flux at modern period or the interstellar radiation field (ISRF) also can be used, which may modify the yield of O-production a little, but the final conclusion holds), the total absorption (δtot)33 and photoionization (δion) cross-sections of H2O, and the quantum yield for forming O-atom photoproducts (O(3P/1D)+2H), Γ, determined in the present work. It is noted that the predissociation rate of H2O is sufficiently fast that the fluorescence quantum yield must be

negligible, so the total photodissociation cross-section will be almost the same as the photoabsorption cross-section. The sigmoidal function through the latter data is used to derive the reported overall O product quantum yield. The quantum yields at l = 111.5 nm, 115.2 nm, 121.57 nm are obtained from Refs. 15, 25 and 27.

Supplementary Files

This is a list of supplementary files associated with this preprint. Click to download.

- ThreeBodyDissociationofWaterSM.docx